JOURNAL OF GEOPHYSICAL RESEARCH: OCEANS, VOL. 118, 1645–1657, doi:10.1002/jgrc.20107, 2013

Increased CO_2 outgassing in February-May 2010 in the tropical Atlantic following the 2009 Pacific El Niño

Nathalie Lefèvre,[1,2] Guy Caniaux,[3] Serge Janicot,[1] and Abdou Karim Gueye[4]

Received 1 August 2012; revised 21 January 2013; accepted 31 January 2013; published 3 April 2013.

[1] The fugacity of CO_2 (fCO_2) has been measured underway during the voyages of a merchant ship sailing from France to Brazil since 2008. High fCO_2 values are observed in 2010, between approximately 8°S and 8°N, and are particularly pronounced in boreal spring. These high values are explained by the anomalous situation occurring in the tropical Atlantic in 2010 after the 2009 El Niño in the Pacific. The weakening of the trade winds during the El Niño event contributes to an increase of sea surface temperatures in the tropical Atlantic and a northward shift of the intertropical convergence zone. The anomalous position of the intertropical convergence zone is accompanied by reduced precipitation in boreal spring and hence a higher than usual sea surface salinity. The year 2010 is also characterized by a strong positive Atlantic multidecadal oscillation index and a negative North Atlantic oscillation index that contribute to the tropical Atlantic warming. Positive anomalies of both surface temperature and salinity cause an increase of surface CO_2, leading to a stronger outgassing of CO_2 in 2010 compared with 2009 and 2011. The main factor responsible for the CO_2 anomalies is the Pacific El Niño teleconnection. The Atlantic multidecadal oscillation index also contributes in the northern hemisphere, and the role of the North Atlantic oscillation is negligible.

Citation: Lefèvre, N., G. Caniaux, S. Janicot, and A. K. Gueye (2013), Increased CO_2 outgassing in February-May 2010 in the tropical Atlantic following the 2009 Pacific El Niño, *J. Geophys. Res. Oceans*, *118*, 1645–1657, doi:10.1002/jgrc.20107.

1. Introduction

[2] The El Niño phenomenon is the dominant mode of interannual variability in the climate system [*Kachi and Nitta*, 1997; *Roeckner et al.*, 1996]. Its impact on the air-sea CO_2 flux has been studied mainly in the tropical Pacific [*Bacastow et al.*, 1980; *Feely et al.*, 1995; *Feely et al.*, 1987; *Fushimi*, 1987; *Inoue and Sugimura*, 1992; *Inoue et al.*, 2001; *Volk*, 1989] where it originates. On the global scale, the strongest interannual variability of the air-sea CO_2 flux is caused by the Pacific El Niño [*Le Quéré et al.*, 2000; *McKinley et al.*, 2004]. The CO_2 distribution in the tropical Pacific during such events has been well documented. The outgassing of CO_2 is significantly reduced during an El Niño event compared with normal years [e.g., *Feely et al.*, 1999; *Inoue and Sugimura*, 1992; *Wong et al.*, 1993]. The equatorial Pacific is the strongest source of CO_2 for the atmosphere because of the upwelling, bringing CO_2-rich waters to the surface and the strong wind speed. During a Pacific El Niño, the reduction of the winds entrains a weakening of the equatorial upwelling that leads to a reduction of the CO_2 outgassing [*Feely et al.*, 1987].

[3] In the tropical Atlantic, two kinds of El Niño phenomena have been reported. One is a consequence of the Pacific El Niño caused by "teleconnection" due to transmission through atmospheric fluctuations described as an atmospheric bridge [*Klein et al.*, 1999]. The tropical Atlantic usually experiences a smaller but anomalous warming several months after the maximum warming in the Pacific, which usually occurs in December [*Enfield and Mayer*, 1997]. The ENSO (El Niño Southern Oscillation) teleconnection to the Atlantic is recognized as a fundamental mode of variability of Atlantic climate [*Saravanan and Chang*, 2000]. It also has an impact on the vertical stabilization of the tropical atmosphere and reduces rainfall over northeast Brazil during the boreal spring [*Giannini et al.*, 2001] as it affects the position of the intertropical convergence zone (ITCZ) [*Chiang et al.*, 2002].

[4] The other kind of Atlantic El Niño effect is a nonsynchronous and aperiodic warming that occurs along the equator and entirely due to internal Atlantic dynamics. It is "El Niño–like" in the sense that the Atlantic dynamics are similar to the Pacific case, but it has no correlation with Pacific events. Moreover, the magnitude of the warming is much smaller than that in the Pacific. This event, sometimes called an Atlantic El Niño, is the leading mode of tropical Atlantic variability with strongest amplitude during May-July [*Deser et al.*, 2010].

[5] The impact of these Atlantic events on the air-sea CO_2 flux is poorly documented because of the paucity of data in this region but also because such events are not very frequent.

[1]IRD LOCEAN, Paris, France.
[2]LaboMar UFC, Fortaleza Brazil.
[3]CNRM/GAME (Météo France/CNRS), Toulouse, France.
[4]LOCEAN, 75252 Paris, France.

Corresponding author: N. Lefèvre, LaboMar UFC, avenida Abolição 3207, 60165-081 Fortaleza-CE, Brazil. (nathalie.lefevre@ird.fr)

2169-9275/13/10.1002/jgrc.20107

[6] A warm event occurred in the tropical Atlantic in boreal winter 1984, following the strong 1982–1983 Pacific El Niño, and was observed during the FOCAL cruises. This event was described as an Atlantic El Niño [*Philander*, 1986]. Warm temperatures were observed in the eastern tropical Atlantic [*Hisard et al*., 1986] and were mostly confined to the equatorial band (5°S–5°N). High values of the seawater fugacity of CO_2 (fCO_2) were associated with the warming effect compared with winters 1982 and 1983, but the reduction of the wind speed occurring during such an event led to air-sea CO_2 fluxes that were not significantly higher than during normal years [*Andrié et al*., 1986]. More recently, *Park and Wanninkhof* [2012] reported a higher CO_2 flux in 2003 in the western tropical Atlantic due to increased sea surface temperatures (SSTs) following the 2002–2003 Pacific El Niño.

[7] The year 2010 is very different from 1984 when examining the indices corresponding to the different modes of SST variability of the Atlantic ocean, such as the Atlantic multidecadal oscillation (AMO), the North Atlantic oscillation (NAO), and the NINO34 (120°W–170°W, 5°S–5°N) for the last 60 years (1952–2011). The year 2010 is characterized by a strong positive AMO index in March-April-May (the strongest index for the period) as well as a negative NAO index in December-January-February (the lowest value for the period) (Figures 1a and 1b). In addition, it follows the 2009 Pacific El Niño, the fourth strongest El Niño for the period 1982–2011 as shown by the index in November-December-January (Figure 1c). In 1984, the AMO index was negative and the NAO was moving to a positive phase.

[8] In this work, we used the regular underway CO_2 measurements made along the shipping line from France to Brazil to document the CO_2 anomalies observed in 2010 and to determine the origin of these anomalies as well as the impact on the air-sea CO_2 flux. First, the anomalies are related to the anomalous physical conditions along the ship track at a local scale. Then, the link between these CO_2 and physical anomalies is examined. As abnormal conditions are observed on the regional (basin) scale on SST and wind fields, the contribution of the AMO and NAO are finally discussed to understand the anomalous conditions observed in 2010 on a much larger scale.

2. Methods and Data

[9] An automated fCO_2 instrument, using infrared detection, similar to the one described by *Pierrot et al*. [2009], has been installed in 2008 on the merchant ship *Monte Olivia* sailing from Le Havre (France) to Santos (Brazil). The *Monte Olivia* follows approximately the same track from one voyage to another (Figure 2), and seawater and atmospheric fCO_2 were measured underway from July 2008 to April 2009. Then the same route was sampled by the *Rio Blanco* from December 2009 onward.

[10] The voyages used in this study are listed in Table 1. The spacing between the northernmost and the southernmost voyages reaches a maximum of 2° in longitude near 15°N–20°N so the spatial variability from one voyage to another can be neglected.

[11] The ship is equipped with a Seabird thermosalinograph SBE 21 recording SST and sea surface salinity (SSS) under way at a depth of 5 m. Here we focus on the fCO_2 data recorded between 15°S and 20°N, indicated by the horizontal bars in Figure 2.

[12] In March 2011, because of problems with the atmospheric pumping on board the merchant ship, no atmospheric fCO_2 measurements could be made. An atmospheric trend of 1.0 µatm/year was estimated from the atmospheric fCO_2 at the Ragged Point station (indicated by a square in Figure 2) that was calculated using the monthly molar fraction of CO_2 from the World Data Centre for Greenhouse Gases Web site and the atmospheric pressure of the NCEP/NCAR reanalysis (National Centers for Environmental Prediction/National

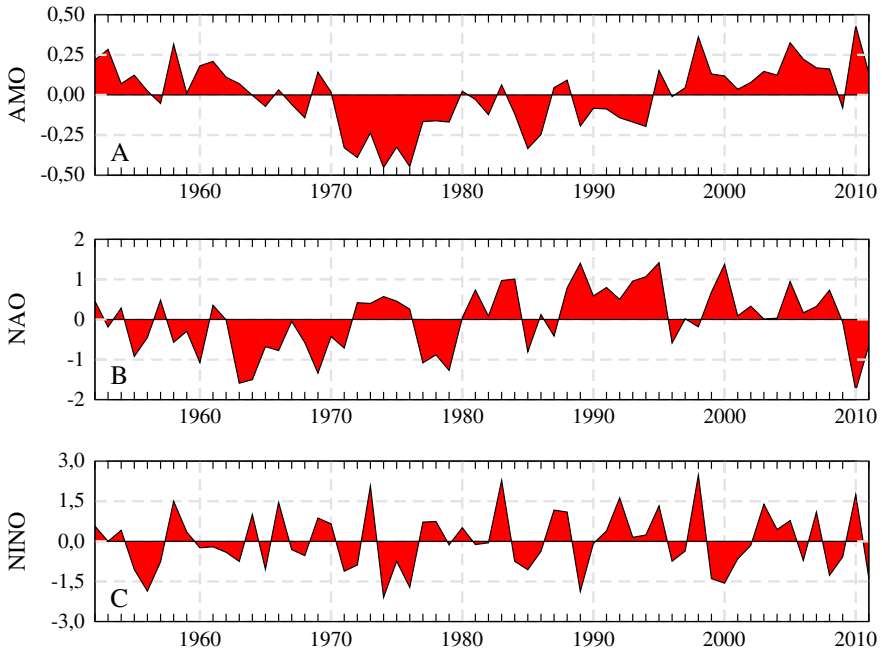

Figure 1. (a) AMO index in March-April-May, (b) NAO index in December-January-February, and (c) NINO34 index in November-December-January for the last 60 years (1952–2011).

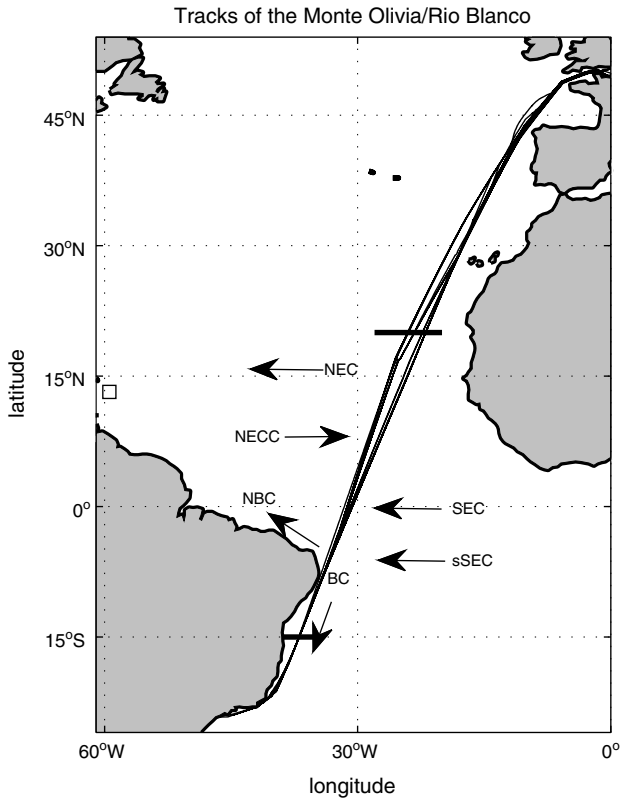

Figure 2. Ship tracks of the *Monte Olivia* and the *Rio Blanco*. The main currents are indicated: the North Equatorial Current (NEC), the North Equatorial Countercurrent (NECC), the South Equatorial Current (SEC), the southern branch of the SEC (sSEC), the North Brazil Current (NBC), and the Brazil Current (BC). The position of the atmospheric station of Ragged Point Barberos is indicated by a square at 13.17°N, 59.43°W. The horizontal lines correspond to the limits of the study area.

Center for Atmospheric Research) project. The same trend was observed with the atmospheric values obtained during the previous voyages of the ship. This trend was added to the atmospheric value of the voyages in March 2010 to estimate the atmospheric values of March 2011.

[13] The air-sea flux of CO_2 (expressed in mmol m^{-2} d^{-1}) is calculated as follows:

$$fCO_2 = K \times So(fCO_{2\,sw} - fCO_{2\,atm}) \quad (1)$$

where $K = 0.27\ u_{10}^2\ (Sc/660)^{-0.5}$ is the gas exchange coefficient given by *Sweeney et al*. [2007] with u_{10} the wind speed at 10 m above sea level; Sc is the Schmidt number; So is the solubility of CO_2 calculated using the formula of *Weiss* [1974]; and fCO_{2sw} and fCO_{2atm} are the fugacity of fCO_2 in seawater and in atmosphere, respectively. A positive flux means a source of CO_2 to the atmosphere.

[14] As the wind speed was not measured on board the ship, u_{10} was taken from the European Centre for Medium-Range Weather Forecasts (ECMWF) reanalysis data set (ERA-interim), which provide a homogeneous time series from 1979 onward [*Dee et al*., 2011]. The analyses, initially at a 0.75° resolution, were downloaded on a grid with a regular horizontal spacing of 0.5° of longitude and 0.5° of latitude. The 6 h wind fields were averaged for the period covered by the ship to cross the equatorial basin (nearly 15 days). The winds were then linearly interpolated at the ship position at the same frequency as the measured parameters (SST, SSS, and fCO_2).

[15] To examine the oceanic conditions at the basin scale, daily SSTs [*Reynolds et al*., 2007] were used from 1982 to 2011. For this 30 year period, daily SST anomalies were computed, averaged for the period taken by the ship to cross the equatorial basin, and interpolated to compute SST anomalies along the ship track. Monthly fields were also deduced from Reynolds' SSTs and ERA-interim winds to get monthly anomalies for the period 1982–2011. To compute the position of the ITCZ, the Global Precipitation Climatology Project (GPCP) [*Adler et al*., 2003; *Xie et al*., 2003] and the Tropical Rainfall Measuring Mission (TRMM) [*Huffman et al*., 2007] daily data sets were used and downloaded from the http://precip.gsfc.nasa.gov/ Web site. The GPCP data (resolution 2.5°) were available from 1979 to 2010, whereas the TRMM data (resolution 0.25°) covered the period 1998 onward.

3. fCO_2, SST, and SSS Variability Along the Ship Track

3.1. Time Evolution of fCO_2 in Different Systems of Currents

[16] The ship crosses different systems of currents along its track from 15°S to 20°N (Figure 2). The southern branch of the South Equatorial Current is a zonal current flowing westward between approximately 25°S and 10°S [*Stramma and Schott*, 1999]. Close to the Brazilian coast, this current bifurcates at approximately 8°S with its water contributing to form the Brazil Current (BC) to the south and the North Brazil Current (NBC) to the north [*Molinari*, 1983]. The SEC has central, equatorial, and northern branches [*Molinari*, 1982; *Stramma and Schott*, 1999], but they are included in the SEC in Figure 2. Further north, the North Equatorial Countercurrent (NECC) lies between the SEC and the NEC and flows eastward. However, because of its meandering features, it is difficult to determine the meridional limits of the NECC [*Urbano et al*., 2008]. According to *Urbano et al*. [2006], the NECC is composed of two cores and is present throughout the year between 3°N and 13°N.

[17] The monthly evolution of fCO_2 has been represented for the regions, including the NEC (13°N–16°N), the NECC (4°N–8°N), the equatorial region (2°S–2°N), the SEC (8°S–4°S), and the BC (15°S–10°S), and the transition between the NBC and the SEC (Figure 3). The range of latitudes for each region has been chosen to represent the main systems of current. In the NEC region, fCO_2 follows the seasonal cycle of SST with higher fCO_2 values in boreal summer and lower values in boreal winter (Figure 3a). The amplitude of the SST is approximately 4°C. North of the equator, in the NECC region, there is no clear seasonal cycle of fCO_2 but the anomaly of fCO_2 is visible in March 2010 (Figure 3b). In the equatorial region (2°S–2°N), there is little seasonal variability, but the CO_2 anomaly observed in 2010 in March is still present (Figure 3c). South of the equator, the water comes from the SEC and forms the NBC; fCO_2 is maximum in March and minimum in July, which corresponds to the seasonal variations of SST. The fCO_2 distribution shows higher values in 2010 than in 2009 and 2011 from March to June (Figure 3d). The variability of fCO_2 in the BC region

Table 1. Voyages of the Merchant Ships (*Monte Olivia* then *Rio Blanco* from December 2009) Along the France-Brazil Line

Dates of the voyages	Minimum latitude	Maximum latitude	Minimum longitude	Maximum longitude	Vessel
12–20 July 2008	18°S	40°N	38°W	12°W	*Monte Olivia*
4–12 August 2008	22°S	42°N	40°W	11°W	*Monte Olivia*
3–13 October 2008	24°S	50°N	44°W	3°W	*Monte Olivia*
14–21 November 2008	4°S	50°N	32°W	3°W	*Monte Olivia*
8–16 December 2008	23°S	51°N	44°W	1°E	*Monte Olivia*
18–28 January 2009	22°S	50°N	41°W	0.5°E	*Monte Olivia*
5–17 February 2009	24°S	50°N	46°W	0.7°W	*Monte Olivia*
1–11 Mar 2009	18°S	52°N	38°W	4°E	*Monte Olivia*
12–22 Apr 2009	21°S	52°N	40°W	4°E	*Monte Olivia*
13–23 December 2009	19°S	50°N	38°W	1°W	*Rio Blanco*
15–25 January 2010	22°S	50°N	41°W	2°W	*Rio Blanco*
7–17 February 2010	22°S	50°N	41°W	0°W	*Rio Blanco*
25 Feb–8 March 2010	22°S	50°N	41°W	0°W	*Rio Blanco*
21–29 March 2010	23°S	43°N	44°W	10°W	*Rio Blanco*
9–22 April 2010	23°S	50°N	41°W	1°W	*Rio Blanco*
6–15 May 2010	23°S	32°S	44°W	17°W	*Rio Blanco*
25 Jun–15 July 2010	23°S	50°N	41°W	0°W	*Rio Blanco*
16–29 July 2010	22°S	50°N	41°W	0°W	*Rio Blanco*
3–16 September 2010	9°S	50°N	34°W	0°W	*Rio Blanco*
24 Oct–4 November 2010	24°S	44°N	46°W	10°W	*Rio Blanco*
17 Nov–1 December 2010	20°S	50°N	39°W	0°W	*Rio Blanco*
18–31 March 2011	23°S	50°N	43°W	1°W	*Rio Blanco*
6–19 May 2011	23°S	49°N	43°W	5°W	*Rio Blanco*
23 Jun–7 July 2011	23°S	50°N	42°W	0°W	*Rio Blanco*

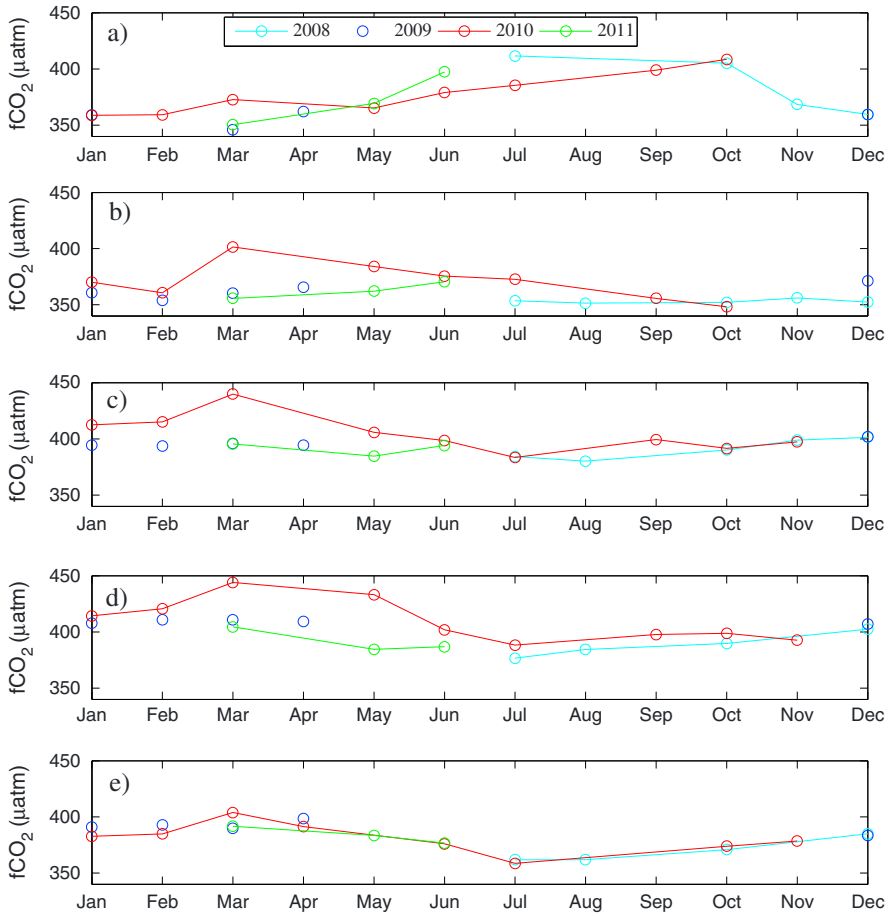

Figure 3. Monthly distribution of the fCO_2 (µatm) in (a) the North Equatorial Current region (13°N–16°N), (b) the North Equatorial Countercurrent region (4°N–8°N), (c) the equatorial region (2°S–2°N), (d) the South Equatorial region (8°S–4°S), and (e) the BC region (15°S–10°S).

shows a minimum in July around 360 µatm and a maximum in March around 390 µatm (Figure 3e). The amplitude of the seasonal cycle is approximately 2.5°C, and the fCO_2 distribution is mainly explained by the temperature variations with minimum values in July-August (austral winter) and maximum values in March (austral summer).

3.2. Latitudinal Distributions of fCO_2

[18] Figure 4 shows the latitudinal distribution of fCO_2 during the voyages of the *Monte Olivia* and the *Rio Blanco* between 15°S and 20°N for each month (Figure 4).

[19] From 15°S to 8°S, fCO_2 is varying between 380 and 400 µatm from December to May and between 360 and 380 µatm from June to November. Higher fCO_2 values are measured during the austral summer, whereas lower fCO_2 values are measured during the austral winter when SSTs are lower, between 26°C and 28°C. At approximately 8°S, where the SEC bifurcates to feed the NBC and the BC, a front of fCO_2 is often observed (Figures 3a–3d and 3f–3j) with lower CO_2 values in the BC. High fCO_2 values are observed in the SEC as it includes the equatorial upwelling. North of the SEC, lower fCO_2 are observed in the NECC, but the transition between the SEC and the NECC is not as abrupt as the front observed in the southern hemisphere near 8°S. The fCO_2 reaches its lowest values near 8°N–10°N. North of this region, in the NEC, the distribution of fCO_2 is variable with higher fCO_2 values of the order of 400 µatm, mainly observed in boreal summer from June to October.

[20] The latitudinal distribution of fCO_2 reproduces more or less the same patterns of CO_2 variability along the track with fronts between the different current systems. However, a significant difference is observed between the year 2010 and the other years. In March 2010, in the SEC, fCO_2 was significantly higher with values reaching 460 µatm (Figures b and 4c). The increase started in February 2010 in the equatorial region (Figures 3c and 4b). The high fCO_2 values persisted during the two voyages made in March 2010 (25 February–8 March and 21–29 March) and were observed in the northern hemisphere as well, up to 8°N. In April and May 2010, the few data available south of the equator suggest that this pattern remains during these months (Figures 4d and 4e). In May 2010, near 5°S, fCO_2 is close to 450 µatm; but in May 2011, it is less than 400 µatm. In June 2010 and 2011, fCO_2 values are close, and the CO_2 anomaly is no longer visible (Figure 4f). In boreal spring 2010, the strong CO_2 anomaly is particularly pronounced between approximately 8°S and 8°N where fCO_2 is much higher than during the other voyages (Figures 4c–4e). The CO_2 anomaly is not observed in the BC and NEC regions (Figures 3a and 3e) and is observed mainly in boreal spring in the SEC and NECC. As the CO_2 anomaly is mainly observed in boreal spring, we focus on the period from January to May to determine the factors that might be responsible for these CO_2 anomalies.

3.3. Latitudinal Distributions of SST and SSS

[21] From January to May (i.e., austral summer), the SSTs are the highest in the southern hemisphere with values higher than 28°C (Figures 5a–5e). From the equator to 20°N, the SST decreases steadily to reach the lowest value at 20°N. In the

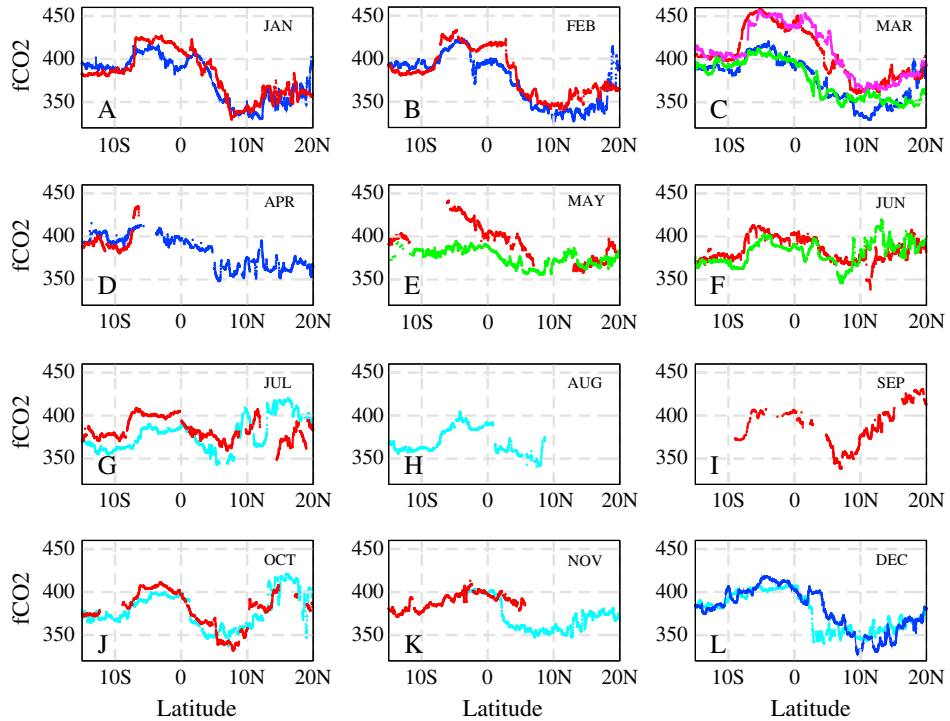

Figure 4. Distribution of the fCO_2 (µatm) as a function of latitude along the ship track for the different months of the years 2008 (cyan), 2009 (blue), 2010 (red) (in March 2010, the red curve is for the beginning and in magenta the end of March) and 2011 (green) for the months of (a) January, (b) February, (c) March, (d) April, (e) May, (f) June, (g) July, (h) August, (i) September, (j) October, (k) November, and (l) December.

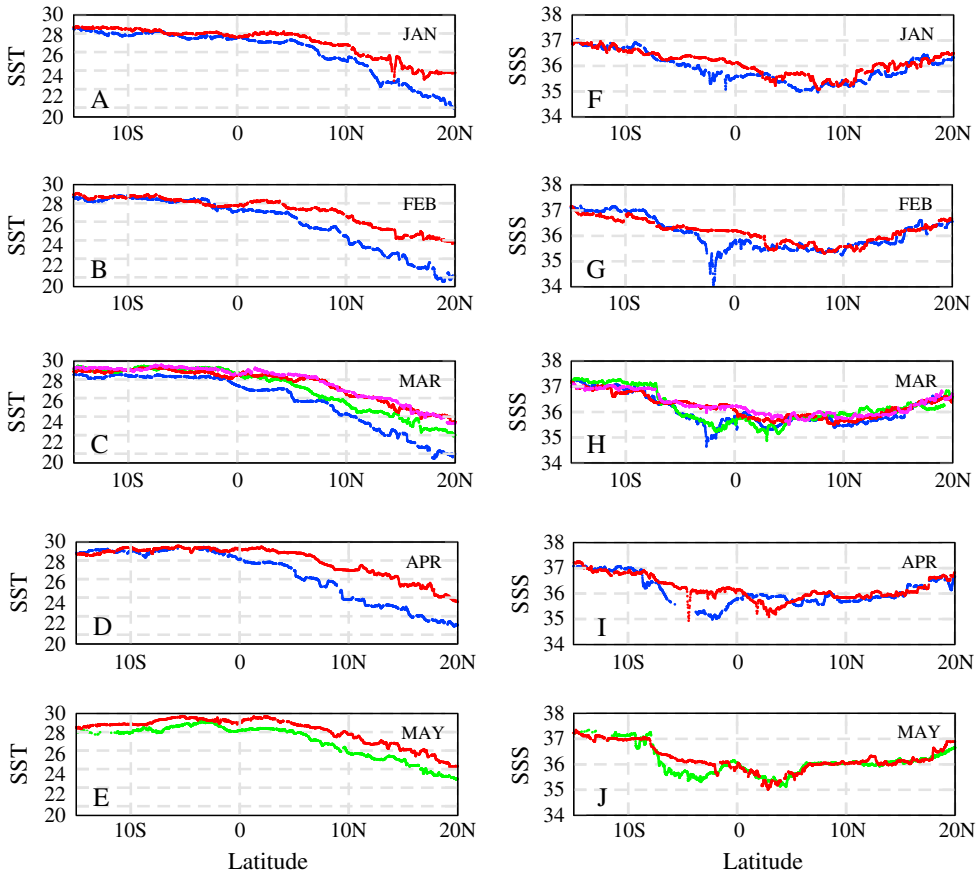

Figure 5. SST distribution (°C) as a function of latitude along the ship track for (a) January, (b) February, (c) March, (d) April, and (e) May. SSS distribution (psu) as a function of latitude for (f) January, (g) February, (h) March, (i) April, and (j) May. The year 2009 is in blue, 2010 is in red, the end of March 2010 is in magenta, and 2011 is in green.

southern hemisphere, there is no significant difference of SST from one year to another, whereas in the northern hemisphere, some significant differences occur between years with a higher SST from January to May in 2010. In January and February, at 20°N, the SST difference reaches 4°C between 2010 and 2009 (Figures a and 5b) and approximately 3°C in April (Figure 5d). In March, south of the equator, the SST is similar in 2010 and 2011 and slightly higher than that in 2009; but in the northern hemisphere, the SST is higher in 2010 compared with 2009 and 2011 (Figure 5c). The SST is slightly higher in May 2010 than that in 2011, with the largest SST difference between 0° and 10°N (Figure 5e).

[22] The distribution of SSS exhibits important differences in 2010 compared with other years. However, unlike the SST, the differences are observed in the southern hemisphere (Figures 5f–5j). From January to May, near 2°S, the salinity decreases in 2009 and 2011 with values lower than 35 in February 2009 (Figure 5g) and in March 2009 (Figure 5h). This salinity decrease is visible in a narrow latitudinal band and is caused by the presence of ITCZ that is generally located south of the equator at this time of the year. One striking feature is the absence of low salinity values in 2010, south of the equator. In April 2010, except a very sharp decrease of salinity (Figure 5i), associated with a sharp cooling (Figure 5d) likely caused by a sudden rain event, the low salinity region is located further north, near 2°N; whereas in 2009, low salinities are observed south of the equator (Figure 5i). In 2010, the salinity remains mostly higher than 36 south of the equator from January to March. In May 2010, the low salinities are located near 4°N. In May 2011, two areas of low salinities are observed, one south of the equator and the other north of the equator (Figure 5j). However, the highest temperature associated with the low salinity south of the equator (Figure 5e) suggests that the ITCZ is located south of the equator in May 2011. From June, the ITCZ moves northward to reach the northernmost latitude of 8°N–10°N, and the low salinity region is found in the northern hemisphere around 8°N–10°N. In boreal summer and northern hemisphere, the salinity distribution does not exhibit strong differences between years.

[23] In the tropical Atlantic, the variability of fCO_2 is affected by salinity changes [*Oudot et al.*, 1995], and low fCO_2 values have been observed in the region of the NECC where high precipitation occurs because of the presence of the ITCZ [*Lefèvre et al.*, 2010; *Oudot et al.*, 1987; *Padin et al.*, 2009]. This mechanism has also been observed in the equatorial Pacific [*Turk et al.*, 2010] and is due to the chemical dilution taking place in these regions.

4. Wind and SST Anomalies Along the Ship Track

4.1. Latitudinal Distribution of Wind and SST Anomalies in 2010

[24] As the CO_2 anomalies are mainly observed in boreal spring, the SST and wind anomalies, calculated for the period 1982–2011, are examined along the ship track from January to May (Figure 6).

[25] Positive SST anomalies are observed along the track of the ship but are more pronounced in the northern hemisphere from 5°N to 20°N (Figures 6a–6e). Between 8°S and 8°N, where the strongest CO_2 anomalies are observed, a positive SST anomaly is smaller than the SST anomalies north of this region. The strongest warming occurs in March 2010 north of 5°N and up to 20°N, with a positive anomaly that can exceed 2°C (Figure 6c). In April and May 2010, the 2°C anomaly is observed further north, from 10°N to 20°N (Figures 6d and 6e).

[26] In addition, the strongest wind anomalies are also observed in the northern hemisphere with the most intense reduction of the winds in February 2010 north of 2°N and up to 20°N (Figure 6g). By March 2010, the wind anomaly is much weaker in the northern hemisphere (Figure 6h). A strong wind anomaly is then observed in April 2010 north of 10°N (Figure 6i), but there is no significant wind anomaly in May 2010 (Figure 6j). A small positive anomaly ranging from 1 to 2 ms^{-1} is present from 5°S to the equator from January to April (Figures 6f–6i).

[27] This suggests that the SST and wind anomalies observed along the ship track are not directly causing the local CO_2 anomalies between 8°S and 8°N as they are located further north of the area of CO_2 anomalies. The SST and wind anomalies are very pronounced in the northern hemisphere, but they are quite weak in the southern hemisphere where strong CO_2 anomalies are observed from 8°S. Therefore, in the southern hemisphere, the main factor associated with the CO_2 anomalies is the high salinity observed in 2010. In addition, the warming of the surface water further increases fCO_2, which explains the high fCO_2 values observed more clearly in March 2010 when the SST anomalies are higher than in January-February between 8°S and 8°N. Although the anomalies are calculated for 30 years, the 2010 anomalies are not significantly different when only the years 2009 and 2011 are used for calculating the anomalies.

4.2. Impact on the Air-Sea Flux of CO_2

[28] A CO_2 anomaly does not necessarily lead to an anomaly of air-sea CO_2 flux because the wind speed needs to be taken into account. If the difference of fCO_2 between the ocean and the atmosphere is large but the wind speed very

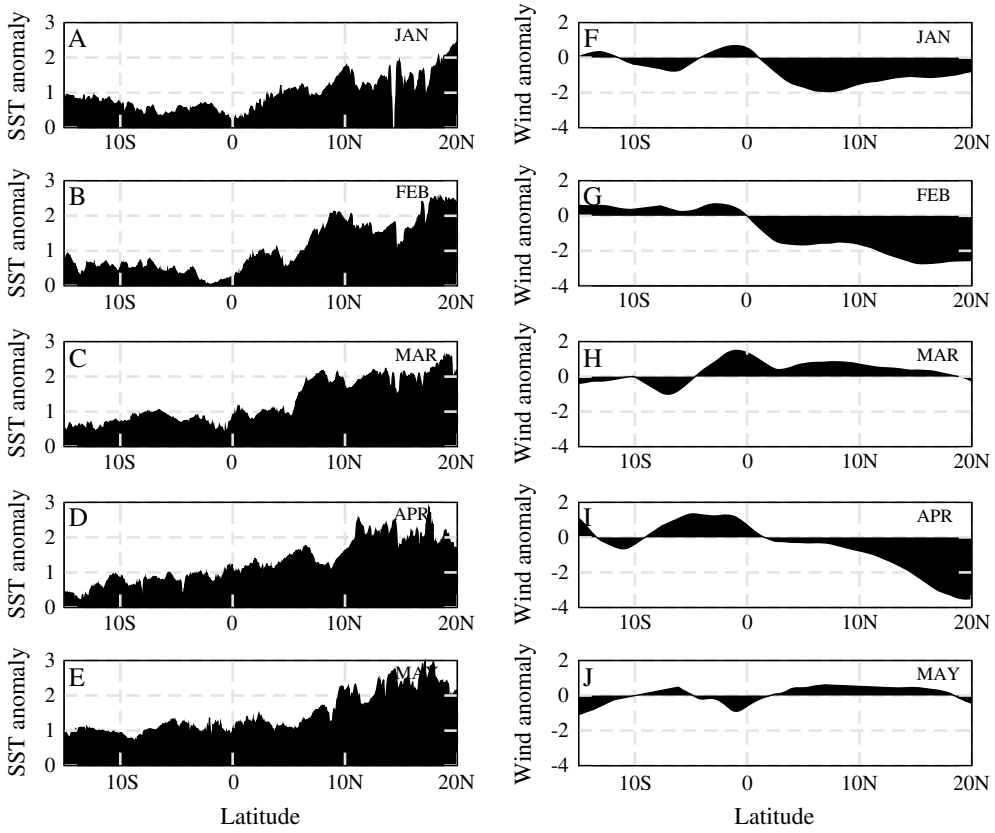

Figure 6. SST anomalies (°C) along the track of the *Rio Blanco* for (a) January, (b) February, (c) March, (d) April, and (e) May 2010. Wind anomalies (ms^{-1}) for (f) January, (g) February, (h) March, (i) April, and (j) May 2010. The SST anomalies are calculated as the difference between the ship SST and the Reynolds SST averaged for 30 years (period 1982–2011) and interpolated at the ship position. The wind anomalies refer to the ECMWF winds minus the 30 year average (period 1982–2011) interpolated at the ship position.

low, the air-sea CO_2 flux will be low. The mean values of the air-sea CO_2 flux in the region 8°S–8°N show that the outgassing was stronger in 2010 (Table 2). In October, the mean CO_2 flux between 8°S and 8°N is very similar in 2010 and 2008. In November, the CO_2 flux is very different between 2008 and 2010. However, this difference could be the result of the lack of data rather than a year to year change. In December, the difference of the CO_2 flux between 2008 and 2009 is explained by the lower fCO_2 observed closer to the equator in 2008 than that in 2009 (Figure 4l). These low fCO_2 are associated with low salinities, which suggests a slight northward position of the ITCZ in December 2009 compared with December 2008.

[29] A stronger CO_2 outgassing is observed in boreal spring 2010 mainly in the northern hemisphere (Figures 7a–7e). Also, the largest difference, in the equatorial band, is observed in March and May (Figures 7c and 7e) during the months of the strongest CO_2 anomalies. From May, there is no anomaly of the CO_2 flux (Figure 7e).

[30] To explain which input parameter of equation (1) leads to a flux anomaly, the contribution of the different parameters to the flux anomaly has been calculated as follows:

Table 2. Mean CO_2 Flux (mmol m^{-2} d^{-1}) Between 8°S and 8°N Along the Ship Track From 2008 to 2011

	January	February	March	April	May	June	July	August	September	October	November	December
2008							0.49	0.67		1.54	1.65[a]	1.20
2009	1.38	1.47	0.85	0.59								2.50
2010	1.77	1.96	4.01 3.04	5.06[a]	2.12[a]	2.17	1.30		1.33	1.53	2.85[a]	
2011			0.52		0.35	1.03						

[a]Significant loss of data within the region 8°S–8°N.

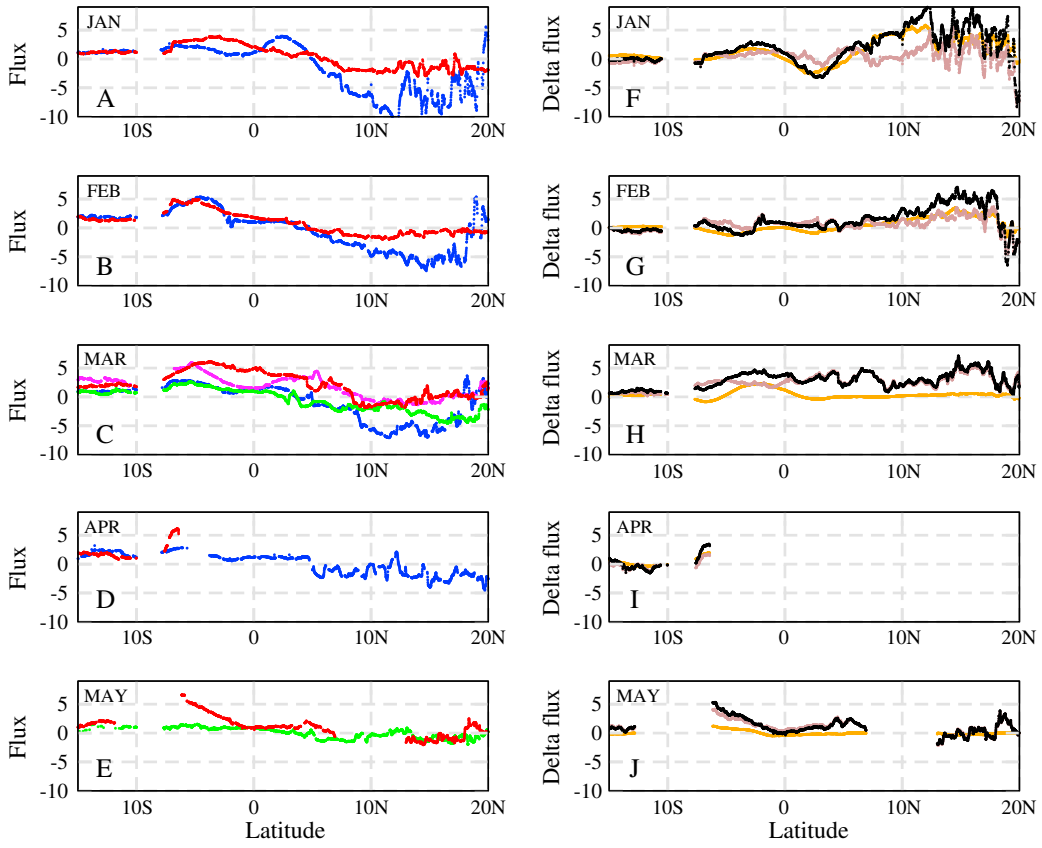

Figure 7. CO_2 flux (mmol m^{-2} d^{-1}) in (a) January, (b) February, (c) March, (d) April, and (e) May for the years 2009 (blue), 2010 (red and magenta for the end of March 2010), and 2011 (green). CO_2 flux anomalies (mmol m^{-2} d^{-1}, black) along the ship track in (f) January, (g) February, (h) end of March, (i) April, and (j) May 2010. The orange curve is the contribution to the flux due to the wind anomaly, and the brown curve is the contribution due to the seawater fCO_2 (the other contributions are negligible and not presented). The anomalies are computed as the difference between the values of SST, SSS, wind, fugacity of atmospheric, and sea water CO_2 in 2010 and the values in other years (i.e., 2009 for January and February, the average between 2009 and 2011 for March, 2009 for April, and 2011 for May).

$$\Delta F = \frac{\partial F}{\partial \mathrm{SST}}\Delta \mathrm{SST} + \frac{\partial F}{\partial S}\Delta S + \frac{\partial F}{\partial u10}\Delta u10 + \frac{\partial F}{\partial fCO_{2\mathrm{atm}}}\Delta fCO_{2\mathrm{atm}} + \frac{\partial F}{\partial fCO_{2\mathrm{sw}}}\Delta fCO_{2\mathrm{sw}} \quad (2)$$

where ΔF is the difference between the flux in 2010 and the flux in other years (i.e., 2009 for January and February, the average between 2009 and 2011 for March, 2009 for April, and 2011 for May). The different contributions to the flux anomaly come from the SST, the salinity (S), the wind speed at 10 m (u_{10}), the atmospheric fCO_2 (fCO_{2atm}), and the seawater fCO_2 (fCO_{2sw}) according to equation (1) used for the calculation of the CO_2 flux.

[31] In January, although the fCO_2 distribution is similar in 2009 and 2010, the CO_2 flux is different with a stronger sink in 2009 than that in 2010 (Figure 7a). Most of the anomaly of the flux is due to the strong reduction of the wind in 2010 (Figure 7f). In January and February 2010, the flux is close to zero in the northern hemisphere due to the weaker winds. In February 2010, the seawater fCO_2 and the wind contribute almost equally (Figure 7g).

[32] In March, the wind anomaly observed in the northern hemisphere is reduced (Figure 6h), and most of the CO_2 flux anomaly is explained by the fCO_2 anomaly (Figure 7h). During this month, the contribution of the wind is close to zero from 5°N to 20°N. In this region, the total CO_2 flux anomaly is fully explained by the contribution of the seawater fCO_2 anomaly as shown by the superposition of the two curves, the total flux anomaly, and the contribution to the flux by the seawater fCO_2 anomalies (Figure 7h). In April, although there are few data, the wind contributes to lower the CO_2 flux south of 10°S, whereas on the CO_2 front, both the wind and the fCO_2 anomalies contribute to the flux anomaly (Figure 7i). In May, close to the CO_2 front, both the wind and the fCO_2 contribute to the flux anomaly with a stronger impact of the fCO_2 anomaly. North of the equator, the wind does not contribute to the CO_2 flux anomaly (Figure 7j), which is consistent with the very low anomalies observed during this month (Figure 6j).

[33] Although there was some wind reduction in 2010, especially in January, February, and April in the northern hemisphere (Figures 6f, 6g, and 6i), overall the CO_2 flux is higher than during normal years because most of the contribution to the CO_2 flux anomaly comes from the seawater fCO_2 anomalies.

5. Origin of the Anomalous Situation in 2010

5.1. The Role of the ITCZ

[34] Low salinities observed south of the equator in boreal winter-spring and located further north from May are explained by the high precipitation associated with the position of the ITCZ that migrates seasonally. The position of the ITCZ is calculated by taking the latitudinal position of the maximum rainfall in the region 35°W–20°W, 10°S–20°N from 1982 to 2010 using the GPCP data as well as the TRMM data from 1998 to 2011 (Figure 8a). The comparison of the two curves shows that the two data sets are in good agreement and that the GPCP series (available from 1982 to 2010) can be mixed to the TRMM series (available from 1998 to 2011) to obtain statistics for the period 1982–2011.

[35] In the western tropical Atlantic, the ITCZ is at its southernmost location in boreal spring (near 2°S) and at its northernmost location in boreal summer (near 10°N). In the beginning of 2010, the position of the ITCZ is shifted northward compared with the other years (Figure 8a), and this is the northernmost position ever reached during the last 30 years. In addition, there is significant reduction of rainfall,

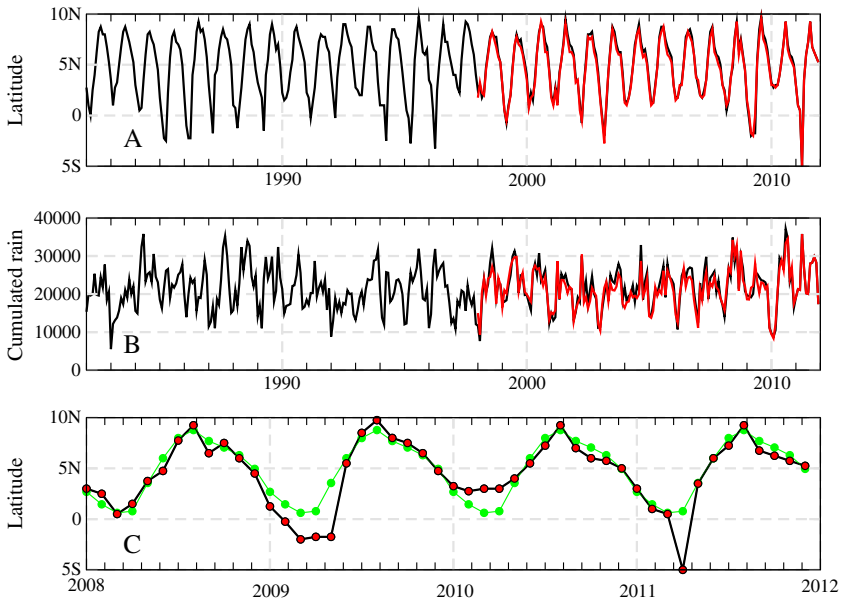

Figure 8. (a) Monthly ITCZ position over the belt 35°W–20°W, (b) monthly cumulated rain (mm/day × grid cells) in the box 35°W–20°W and 10°S–20°N. The black curve is obtained with the GPCP data set (period 1982–2010) and the red curve with the TRMM data set (period 1998–2011). (c) Zoom of the monthly position of the ITCZ from 2008 to 2011 (black curve with red dots) with the mean position of the ITCZ for 30 years (green).

calculated over the same box as for the ITCZ position (Figure 8b representing the precipitation rates cumulated in time and over the grid cells of the target area). In 2010, the cumulated rain rate is lower than usual, particularly in boreal spring with cumulated values less than 10000 mm/day. By examining more closely the position of the ITCZ between 2008 and 2011, it appears that the anomalous position of the ITCZ in 2010 is observed in boreal spring (from January to April) when the ITCZ is located further north compared with the years 2008, 2009, and 2011 as well as to the mean position of the ITCZ for 30 years (Figure 8c). In March 2008, the ITCZ is close to the equator, and it is south of the equator in March 2009 and April 2011. However, there is no position anomaly in boreal summer when the ITCZ migrates to reach its northernmost position. The ITCZ position in 2010 is at the same location as the ITCZ in other years, close to 10°N in August. The anomaly of the ITCZ position in 2010 is only seen in boreal spring when the ITCZ remains in the northern hemisphere, near 2°N.

[36] The presence of the ITCZ coincides well with the low salinities observed during the voyages of the *Monte Olivia* and *Rio Blanco*. Salinity is generally close to 35 in boreal spring but can decrease down to 34 as in February 2009 (Figure 5g). However, in 2010, the salinity remains higher than 36 in the southern hemisphere from January to May (Figures 5f–5j), consistent with the northward shift of the ITCZ. Although the ITCZ is located further north, near 3°N, in boreal spring 2010 (Figure 8c), there is no significant decrease of salinity associated with the ITCZ (Figures 5g and 5h), which can be explained by the significant reduction of precipitation during that period (Figure 8b). From July 2010, the cumulated rain rate and the position of the ITCZ are similar to the ones observed during the years 2009 and 2011.

[37] The northward shift of the ITCZ and the reduction of precipitation explain the anomalous distribution of salinity in 2010 in the southern hemisphere. However, SST anomalies are also observed along the ship track from the equator up to 20°N, mainly from February to April 2010.

5.2. Basin-Scales Distributions of SST and Winds

[38] The distribution of SST in February-March-April 2010 is shown in Figure 9a. SST anomalies are calculated as the difference of SST between February-March-April minus the SST for the period 1982–2011 for the Atlantic basin from 20°S to 35°N (Figure 9b). The anomalous warming is spread throughout the tropical North Atlantic with the highest SST anomalies close to the African coast near 20°N in the region where a strong meridional SST gradient is observed (Figure 9a). South of the equator, there is a slight warming, but the SST anomalies are much weaker than that in the northern hemisphere.

[39] The warmer SSTs might be explained by weaker winds in 2010. The wind distribution in February-March-April 2010 is shown in Figure 9c with the position of the ITCZ determined by the rain rate from the GPCP data for the same period. The ITCZ is located at the convergence of the northeast (NE) trade winds and the southeast (SE) trade winds. The wind anomalies show a strong reduction of the NE trade winds and a slight increase of the SE trade winds crossing the equator (Figure 9d). The zonal component of the SE trade winds is stronger between 5°S and 1°N. In addition, the meridional component of the NE trade winds is weaker from 1°S to 10°N. The two effects lead to a weaker convergence of the

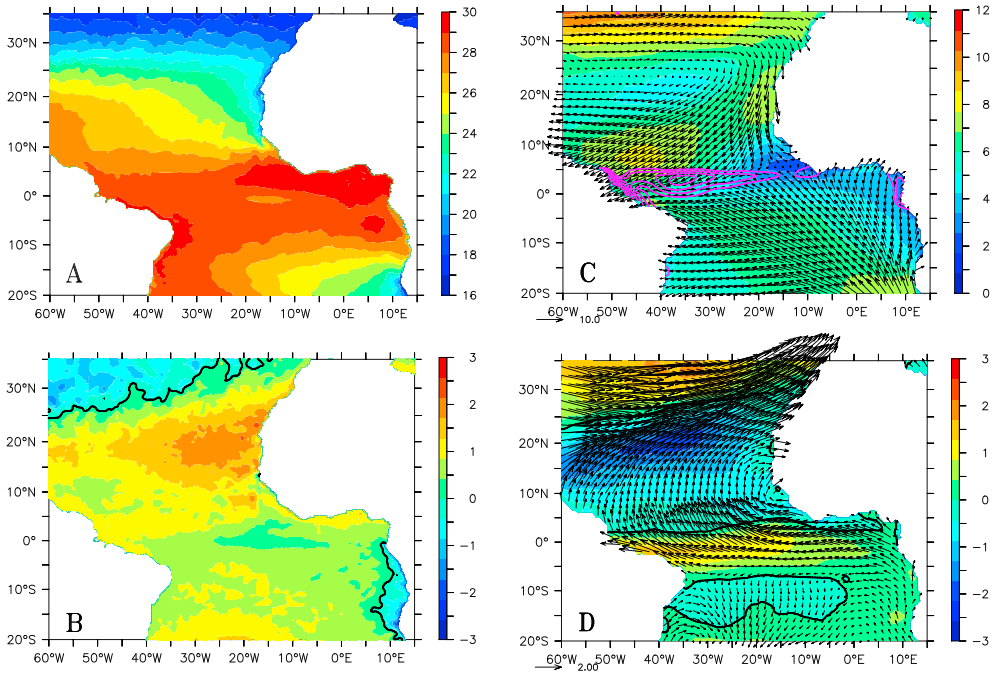

Figure 9. (a) Reynolds' SST (°C), (b) SST anomalies (°C) during the period February-March-April 2010 compared with the average for 1982–2011 (the thick black line represents the iso-0), and (c) ECMWF winds (colors and arrows in ms^{-1}) with the ITCZ position (magenta). Isolines are from 5 to 10 mm/day every mm/day. (d) ECMWF winds anomalies (colors and arrows in ms^{-1}) during the period February-March-April 2010 compared with the February-March-April average for 1982–2011.

trade winds, causing a reduction of precipitation. The weakening of the NE trade and the strengthening of the SE winds cause the northward displacement of the ITCZ.

[40] The anomalous situation in the tropical Atlantic is particularly pronounced in boreal spring and follows the Pacific El Niño of 2009. Warm temperature anomalies can be caused by a relaxation of the winds during the transition from El Niño to La Niña events [*Deser et al.*, 2010]. The situation in 2010 corresponds to what is described as a teleconnection mechanism between the Pacific and the Atlantic oceans via the atmospheric bridge [*Wang*, 2005]. A similar situation was observed in 2003 by *Park and Wanninkhof* [2012], using repeated transects of the ship *Explorer of the Seas* equipped with an automated CO_2 system. Following the Pacific El Niño of 2002–2003, they observed higher SST in the region 19°N–20°N, 65°W–68°W in boreal winter that led to higher seawater fCO_2 and a source of CO_2 in a region that is normally a sink of CO_2.

6. Larger-Scale Processes Contributing to the 2010 Abnormal Conditions

[41] It is still not clear why some Pacific El Niño events are not followed by warm anomalies in the tropical Atlantic [*Wang*, 2005]. One possible explanation could be the impact of other factors such as the AMO and/or the NAO. The AMO is an indicator of the meridional overturning circulation (MOC) and is characterized by a north-south temperature gradient. The positive AMO leads to higher temperature in the northern hemisphere. In 2010, a strong positive AMO is observed (Figure 1a). Combined with a reduction of wind speed following the 2009 El Niño, the positive AMO would reinforce the SST anomalies in the northern tropical Atlantic. The NAO pattern on the ocean consists of an SST tripole. In a negative NAO phase, the SST will increase in northern high latitudes, decrease at moderate latitudes, and increase in the tropical band. In 2010, the NAO is in a negative phase, which contributes to increase the SST in the tropical band. Therefore, the three indices (AMO, NAO, and NINO34) contribute to increase the SST in the northern tropical Atlantic.

[42] To better discriminate the possible influence of each index on the abnormal year 2010, a statistical analysis has been performed. An SST index (SSTA) and a wind index (Wind) were computed from the mean monthly SSTs and winds over the box 50°W–20°W 5°N–25°N and in April (i.e., where and when the anomalies of SST and wind are the strongest). An index characterizing the ITCZ position was also calculated as well as an index of rainfall rate (RR) over the box 35°W–20°W 10°S–20°N for the period February-March-April (in the same way as in Figure 7a).

[43] Scatterplots of AMO, NAO, and NINO34 were performed for the period 1982–2011. The scatterplot of SSTA as a function of AMO versus NINO34 is presented in Figure 10a, as well as a function of AMO and NAO in Figure 10b. The warmest years (SSTA > quintile 4) have a positive AMO index and a positive NINO34 index; however, the year 2011 has a negative NINO34, and one can find years for all the quintiles with positive NINO34. Some dependency appears between these two indices that are positively correlated (see below). In Figure 10b, no clear pattern is observed for the warmest years in relation with NAO: the warmest years can be observed either in a positive phase or in a negative

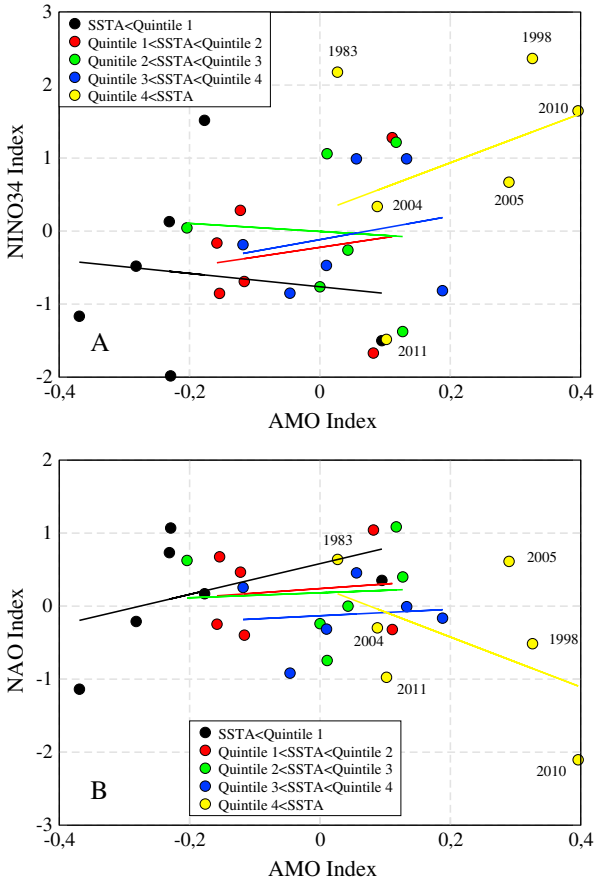

Figure 10. (a) Scatterplot of the SST index, SSTA, as a function of the NINO34 index versus AMO index. (b) Scatterplot of the SST index as a function of the NAO index versus AMO index. The series of SST indices is split into quintiles, and the warmest years are indicated in yellow (SSTA > Quintile 4). The regression lines are indicated for each quintile.

phase of the NAO. The year 2010 corresponds to a strong negative NAO index.

[44] Multiple linear regression models have been computed to estimate separately these four indices with the combinations of AMO, NAO, and NINO34 indices (predictors). The significance of the regression coefficients has been evaluated, highlighting the predictors that have an impact within the multiple regression estimates of the four indices (Table 3). The multiple correlation coefficients are also indicated in the last column of Table 3. The results confirm what characterizes 2010 and shows that AMO, NAO, and NINO34 induce consistent impacts: within the multiple regression modeling, SSTA is explained highly by the AMO (positively) and also by the NAO (negatively), Wind by NINO34 (negatively), ITCZ by AMO (positively), and RR by NINO34 (negatively); so in 2010, the positive phase of AMO contributes significantly to warmer SST (as well as the negative phase of the NAO does) in the SSTA area and to a more northward ITCZ (leading to lower rainfall in the *RR* area). The positive phase of NINO34 contributes to weaker winds in the wind area (enhancing the increase of SSTA) and to weaker rainfall in the *RR* area.

[45] In terms of individual linear correlations (not shown), AMO, NAO, and NINO34 are weakly dependent, except a

Table 3. Regression Coefficients Associated to AMO, NAO, and NINO34 for Each Multiple Regression Model Used to Estimate the Indices SSTA, Wind, ITCZ, and RR[a]

	AMO	NAO	NINO34	Multiple correlation
SSTA	+2.0 (2×10^{-6})	−0.16 (5×10^{-2})	—	+0.85
Wind	—	—	−0.16 (4×10^{-2})	+0.44
ITCZ	+3.21 (4×10^{-2})	—	—	+0.49
RR	—	—	−1251.3 (3×10^{-2})	+0.48

[a]The statistical significance level of these coefficients is provided in parenthesis; only coefficients whose levels are better than 5% (5×10^{-2}) are indicated. The multiple correlation coefficients are indicated in the last column; they are all significant at least at the 2% level.

positive correlation between AMO and NINO34 significant at the 5% statistical level. On the other hand, SSTA is negatively correlated with Wind (1% level) and positively with ITCZ (1% level), and ITCZ is negatively correlated with RR (1% level). Notice also that, within the multiple regression models, first, the impact of AMO on SSTA is by far the highest in all the relationships; and second, the impact of NINO34 on SSTA is not significant because NINO34 is correlated with AMO and does not provide any significant complementary information while NAO does.

[46] Most of the SST anomalies observed in the tropical North Atlantic in boreal spring are due to the strong positive AMO index and to a least extent to NAO; the Pacific El Niño teleconnection with the Atlantic can also contribute through the wind speed decrease. Another feature of the El Niño teleconnection is the rainfall decrease (Table 3), which plays an important role in the CO_2 anomalies as higher salinities than usual are observed in the southern hemisphere leading to higher fCO_2 without significant increase of SST. It is also worth noting that although strong temperature anomalies are observed in the northern hemisphere, the strongest CO_2 anomalies are not collocated with them but occur mainly in the equatorial band. The NAO has been found to play a significant role in the interannual variability of the air-sea CO_2 flux in the North Atlantic near Bermuda [*Bates*, 2007] and at ESTOC, the European time-series in the Canary Islands [*Santana Casiano et al.*, 2007], but its role is negligible in the CO_2 anomalies observed in 2010 in the equatorial Atlantic.

7. Conclusions

[47] The fCO_2 distribution measured underway along the France-Brazil shipping line shows a CO_2 anomaly in 2010 between approximately 8°S–8°N in boreal spring. That year was characterized by a strong positive AMO index, a negative NAO index, and follows the Pacific El Niño of 2009, the fourth strongest for the 1982–2011 period. AMO and to a less extent NAO and NINO34 contribute to increase the SST in the northern tropical Atlantic. In the southern hemisphere, a northward shift of the ITCZ position in 2010 associated with a reduction of precipitation leads to higher surface salinity, which is associated with the higher fCO_2 observed in boreal spring in the southern hemisphere. NINO34 and AMO contribute to this pattern.

[48] The previous interannual variability of fCO_2 in the tropical Atlantic was reported for the year 1984 after the strong Pacific El Niño of 1982–1983. The 1984 and 2010 events show significantly different distribution of fCO_2 as well as different SST patterns. In 1984, the SST anomalies are mainly observed in the equatorial band in the eastern Atlantic. This event was described as an "Atlantic El Niño" and did not lead to SST anomalies in the western tropical Atlantic. In 1984, the AMO was negative (Figure 1a), which contributed to decrease the SST in the northern tropical Atlantic. In 1984, the air-sea CO_2 flux was not significantly different from normal years [*Andrié et al.*, 1986]. In 2010, the outgassing is stronger than during normal years. The flux is mainly driven by the CO_2 anomaly as the reduction of wind speed, occurring during the anomalous conditions, does not counterbalance the difference of fCO_2 between the ocean and the atmosphere.

[49] As proved by the data used in this study, regular monitoring of CO_2 in the ocean can document and investigate the interannual variability of the air-sea CO_2 flux. Although 2010 was particularly abnormal, the occurrence of El Nino teleconnection in the tropical Atlantic will increase the CO_2 flux, as the main driver for the high fCO_2 observed is the reduction of rainfall caused by the northward shift of the ITCZ. These events are likely to occur in the near future due to more frequent El Niños since the last 10 years [*McPhaden et al.*, 2011]. Maintaining the CO_2 monitoring programs will allow us to gain more insights into the link between the climate variability and the CO_2 exchange across the air-sea interface as well as the mechanisms driving the CO_2 variability.

[50] **Acknowledgments.** This work was funded by the European Integrated Project CARBOCHANGE (FP7 264879), the Institut de Recherche pour le Développement (IRD), and the national program LEFE CYBER. The authors are very grateful to Denis Diverrès for taking in charge the CO_2 measurements on board the merchant ships and to the US IMAGO of IRD for its technical support. They are also grateful to two anonymous reviewers for providing thorough and constructive comments on the manuscript and to Miguel Goni and the JGR-Oceans Associate Editor for evaluating our work.

References

Adler, R. F., et al. (2003), The version 2 Global Precipitation Climatology Project (GPCP) Monthly Precipitation Analysis (1979–Present), *J. Hydrometeorol.*, *4*, 1147–1167.

Andrié, C., C. Oudot, C. Genthon, and L. Merlivat (1986), CO_2 fluxes in the tropical Atlantic during FOCAL cruises, *J. Geophys. Res.*, *91*(C10), 11,741–711,755.

Bacastow, R. B., J. A. Adams, C. D. Keeling, D. J. Moss, and T. P. Whorf (1980), Atmospheric carbon dioxide, the Southern Oscillation, and the weak 1975 El Niño, *Science*, *210*, 66–68.

Bates, N. (2007), Interannual variability of the oceanic CO_2 sink in the subtropical gyre of the North Atlantic Ocean over the last 2 decades, *J. Geophys. Res.*, *112*(C09013), doi:10.1029/2006JC003759.

Chiang, J. C. H., Y. Kushnir, and A. Giannini (2002), Deconstructing Atlantic Intertropical Convergence Zone variability: Influence of local cross-equatorial sea surface temperature gradient and remote forcing from eastern equatorial Pacific, *J. Geophys. Res.*, *107*(D1, 4004), doi:10.1029/2000JD000307.

Dee, D. P., et al. (2011), The ERA-interim reanalysis: configuration and performance of the data assimilation system, *Q. J. R. Meteorolog. Soc.*, *137*, 553–597.

Deser, C., M. A. Alexander, S.-P. Xie, and A. S. Phillips (2010), Sea surface temperature variability: patterns and mechanisms, *Annu. Rev. Mar. Sci.*, *2*, 115–143.

Enfield, D. B., and D. A. Mayer (1997), Tropical Atlantic variability and its relation to El Niño Southern Oscillation, *J. Geophys. Res.*, *102*(C1), 929–945.

Feely, R. A., R. H. Gammon, B. A. Taft, P. E. Pullen, L. S. Waterman, T. J. Conway, J. F. Gendron, and D. P. Wisegarver (1987), Distribution of chemical tracers in the eastern equatorial Pacific during and after the 1982–1983 El Niño/Southern Oscillation event, *J. Geophys. Res.*, *92*(C6), 6545–6558.

Feely, R. A., R. Wanninkhof, C. E. Cosca, P. Murphy, M. F. Lamb, and M. D. Steckley (1995), CO_2 distributions in the equatorial Pacific during the 1991–1992 ENSO event, *Deep Sea Res. Part II*, *42*(2–3), 365–386.

Feely, R. A., R. Wanninkhof, T. Takahashi, and P. P. Tans (1999), Influence of El Niño on the equatorial Pacific contribution to atmospheric CO_2 accumulation, *Nature*, *398*, 597–601.

Fushimi, K. (1987), Variation of carbon dioxide partial pressure in the western North Pacific surface water during the 1982/83 El Niño event, *Tellus*, *39B*, 214–227.

Giannini, A., J. C. H. Chiang, M. A. Cane, Y. Kushnir, and R. Seager (2001), The ENSO teleconnection to the tropical Atlantic ocean: contributions of the remote and local SSTs to rainfall variability in the tropical Americas, *J. Clim.*, *14*, 4530–4544.

Hisard, P., C. Hénin, R. W. Houghton, B. Piton, and P. Rual (1986), Oceanic conditions in the tropical Atlantic during 1983 and 1984, *Nature 322*, 243–245.

Huffman, G. J., R. F. Adler, D. T. Bolvin, G. Gu, E. J. Nelkin, K. P. Bowman, E. F. Stocker, and D. B. Wolff (2007), The TRMM multi-satellite precipitation analysis: quasi-global, multi year, combined-sensor precipitation estimates at fine scale, *J. Hydrometeorol.*, *8*, 33–55.

Inoue, H. Y., and Y. Sugimura (1992), Variations and distributions of CO_2 in and over the equatorial Pacific during the period from the 1986/87 El Niño event to the 1988/89 La Niña event, *Tellus*, *44B*, 1–22.

Inoue, H. Y., et al. (2001), Distributions and variations in the partial pressure of CO in surface waters (pCO_2^w) of the central and western equatorial Pacific during the 1997/1998 El Niño event, *Mar. Chem.*, *76*, 59–75.

Kachi, M., and T. Nitta (1997), Decadal variations of the global atmosphere–ocean system, *J. Meteorol. Soc. Jpn.*, *75*(3), 657–675.

Klein, S. A., B. J. Soden, and N.-C. Lau (1999), Remote sea surface temperature variations during ENSO: evidence for a tropical atmospheric bridge, *J. Clim.*, *12*, 917–932.

Le Quéré, C., J. C. Orr, P. Monfray, O. Aumont, and G. Madec (2000), Interannual variability of the oceanic sink of CO_2 from 1979 through 1997, *Global Biogeochem. Cycles*, *14*(4), 1247–1266.

Lefèvre, N., D. Diverrès, and F. Gallois (2010), Origin of CO_2 undersaturation in the western tropical Atlantic, *Tellus B*, *62*(5), 595–607.

McKinley, G. A., C. Rödenbeck, M. Gloor, S. Houweling, and M. Heimann (2004), Pacific dominance to global air-sea CO_2 flux variability: A novel atmospheric inversion agrees with ocean models, *Geophys. Res. Lett.*, *31* (L22308), doi:10.1029/2004GL021069.

McPhaden, M. J., T. J. Lee, and D. McClurg (2011), El Niño and its relationship to changing background conditions in the tropical Pacific Ocean, *Geophys. Res. Lett.*, *38*(LI5709), doi:10.1029/2011GL048275.

Molinari, R. L. (1982), Observations of eastward currents in the tropical South Atlantic Ocean: 1978–1980, *J. Geophys. Res.*, *87*(C12), 9707–9714.

Molinari, R. L. (1983), Observations of near-surface currents and temperature in the central and western tropical Atlantic ocean, *J. Geophys. Res.*, *88*(C7), 4433–4438.

Oudot, C., C. Andrié, and Y. Montel (1987), Evolution du CO_2 océanique et atmosphérique sur la période 1982–1984 dans l'Atlantique tropical, *Deep Sea Res.*, *34*(7), 1107–1137.

Oudot, C., J. F. Ternon, and J. Lecomte (1995), Measurements of atmospheric and oceanic CO_2 in the tropical Atlantic: 10 years after the 1982–1984 FOCAL cruises, *Tellus*, *47B*, 70–85.

Padin, X. A., et al. (2009), Air-sea CO_2 fluxes in the Atlantic as measured during the FICARAM cruises, *Biogeosci. Discuss.*, *6*, 5589–5622.

Park, G.-H., and R. Wanninkhof (2012), A large increase of the CO_2 sink in the western tropical North Atlantic from 2002 to 2009, *J. Geophys. Res.*, *117*(C080029), 10.1029/2011JC007803.

Philander, S. G. H. (1986), Unusual conditions in the tropical Atlantic Ocean in 1984, *Nature*, *332*, 236–238.

Pierrot, D., C. Neill, K. Sullivan, R. Castle, R. Wanninkhof, H. Lüger, T. Johannessen, A. Olsen, R. A. Feely, and C. E. Cosca (2009), Recommendations for autonomous underway pCO_2 measuring systems and data-reduction routines, *Deep Sea Res.*, *56*, 512–522.

Reynolds, R. W., T. M. Smith, C. Liu, D. B. Chelton, K. S. Casey, and M. G. Schlax (2007), Daily high resolution blended analysis for sea surface temperature, *J. Clim.*, *20*, 5473–5496.

Roeckner, E., J. M. Oberhuber, A. Bacher, M. Christoph, and I. Kirchner (1996), ENSO variability and atmospheric response in a global coupled atmosphere–ocean GCM, *Clim. Dyn.*, *12*, 737–754.

Santana Casiano, J. M., M. Gonzalez Davila, M. J. Rueda, O. Llinas, and E.-F. Gonzalez Davila (2007), The interannual variability of oceanic CO2 parameters in the northeast Atlantic subtropical gyre at the ESTOC site, *Global Biogeochem. Cycles*, *21*(GB1015), doi:10.1029/2006GB002788.

Saravanan, R., and P. Chang (2000), Interaction between tropical Atlantic variability and El Niño-southern oscillation, *J. Clim.*, *13*, 2177–2194.

Stramma, L., and F. Schott (1999), The mean flow field of the tropical Atlantic Ocean, *Deep Sea Res. Part II*, *46*, 279–303.

Sweeney, C., E. Gloor, A. R. Jacobson, R. M. Key, G. McKinley, J. L. Sarmiento, and R. Wanninkhof (2007), Constraining global air-sea gas exchange for CO_2 with recent bomb ^{14}C measurements, *Global Biogeochem. Cycles*, *21*, doi:10.1029/2006GB002784.

Turk, D., C. J. Zappa, C. S. Meinen, J. R. Christian, D. T. Ho, A. G. Dickson, and W. R. McGillis (2010), Rain impacts on CO_2 exchange in the western equatorial Pacific Ocean, *Geophys. Res. Lett.*, *37*(L23610), doi:10.1029/2010GL045520.

Urbano, D. F., M. Jochum, and I. C. A. Da Silveira (2006), Rediscovering the second core of the Atlantic NECC, *Ocean Modell.*, *12*(1–2), 1–15.

Urbano, D. F., R. A. F. De Almeida, and P. Nobre (2008), Equatorial Undercurrent and North Equatorial Countercurrent at 38°W: a new perspective from direct velocity data, *J. Geophys. Res.*, *113*(C04041), doi:10.1029/2007JC004215.

Volk, T. (1989), Effect of the equatorial Pacific upwelling on atmospheric CO_2 during the 1982–1983 El Niño, *Global Biogeochem. Cycles*, *3*(3), 267–275.

Wang, C. (2005), ENSO, Atlantic climate variability, and the walker and hadley circulation, in The Hadley circulation: present, past and future, edited by H. F. Diaz and R. S. Bradley, pp. 173–202, Kluwer Academic Publishers, Netherlands.

Weiss, R. F. (1974), CO_2 in water and seawater: the solubility of a non-ideal gas, *Mar. Chem.*, *2*, 203–215.

Wong, C. S., Y.-H. Chan, J. S. Page, G. E. Smith, and R. D. Bellegay (1993), Changes in equatorial CO_2 flux and new production estimated from CO_2 and nutrient levels in Pacific surface waters during the 1986/87 El Niño, *Tellus*, *45B*, 64–79.

Xie, P., J. E. Janoviak, P. A. Arkin, R. F. Adler, A. Gruber, R. Ferraro, G. J. Huffman, and S. Curtis (2003), GPCP pentad precipitation analyses: an experimental data set based on gauge observations and satellite estimates, *J. Clim.*, *16*, 2197–2214.